Supramolecular Capsules

Solution-Phase Magnetic Mechanistic Study of Ni-Seamed Pyrogallol[4]arene Nanocapsules Reveal Presence of Novel Cylindrical and Spherical Species

Harshita Kumari,* Cindi L. Dennis, Steven R. Kline, Andrew V. Mossine, Carol A. Deakyne, and Jerry L. Atwood*

Abstract: The magnetic properties of nickel-seamed *C*-pyrogallol[4]arene (PgC_3Ni) hexamers and dimers are studied for the first time in solution. The combination of small-angle neutron scattering and superconducting quantum interference device magnetometer measurements of the solution species reveal their paramagnetic and weakly antiferromagnetic behaviour. Surprisingly, the magnetic results indicated the presence of an unprecedented 13 Å-radius species, larger than both the dimeric and hexameric nanocapsules with both octahedral and square-planar metal centers. To confirm the presence of this novel species, we performed a mechanistic study of PgC_3Ni as a function of temperature and solvent and deduced the presence of two additional new species: a) an 11 Å cylinder with Ni atoms seaming the tubular framework and b) an 8 Å-radius sphere with non-interacting Ni centers located within the internal cavity. Select parameters that shift the equilibrium towards desired species are also identified.

One of the foundations of supramolecular chemistry is the visualization that solid-state structures give to solution-phase behavior. Determining specific changes in the shape, size, and other properties of supramolecular assemblies in solution as compared to the solid state has been a challenging task. Insight into solution behavior has been

obtained through techniques such as light scattering and diffusion nuclear magnetic resonance (NMR).[1–3] Although the latter is clearly a powerful technique, it lacks the ability to disclose the details of complex assemblies in solution. Significant details about such structures can be obtained by small-angle neutron scattering (SANS) measurements with modelling and data analysis.[4,5] SANS is a powerful tool that can provide geometric dimensions of species in solution as well as possible interactions between those species.[6]

In this work, SANS measurements have been interwoven with superconducting quantum interference device (SQUID) magnetometry to explore the solution-phase architecture and magnetic properties of nickel-seamed *C*-propylpyrogallol[4]arene (PgC_3Ni) nanocapsules in solution. Our previous investigations have disclosed the solid-state structures of PgC_3Ni dimeric and hexameric nanocapsules.[7] These nanocapsular entities self-assemble employing 8 and 24 nickel ions with 2 and 6 PgC_3 macrocycles, respectively, to form the dimeric and hexameric frameworks (Figure 1). The metal (M) atoms in a dimer are arranged in an equatorial fashion to yield M···M distances of ≈ 4 Å and square pyramidal Oxygen-Metal-Oxygen (O–M–O) bond angles of $\approx 151°$. On the other hand, the hexameric self-assembled entity is composed of 8 $(O–M–O)_3$ octahedral metal triads with a similar M···M distance of ≈ 4 Å in a given triad and a similar M···M distance of ≈ 10 Å between adjacent triads of metal atoms. The O–M–O bond angle of 98.9° in the hexamer adds to the differences in the structural features of the two types of nanocapsules.[7]

In addition to the differences in M···M distances and O–M–O bond angles, the octahedral arrangement of nickel ions in the hexamers versus the square pyramidal arrangement in the dimers prompted questions pertaining to the differences in the stability and magnetic properties of these assemblies in solution. These possible differences propelled us to perform a cohesive solution-phase magnetic and stability study that excitingly revealed the presence of previously unidentified species along with the dimers and hexamers.

Our initial step in this investigation involved comparing the sizes of the nickel-seamed *C*-propylpyrogallol[4]arene nanocapsules in the solid versus the solution phase. The rationale for this step was to ensure the similarity in the geometric dimensions of the dimeric and hexameric nanocapsules in the two phases. SANS data analyses for the hexamers in solution revealed the presence of spherical

[*] Prof. H. Kumari
James L. Winkle College of Pharmacy, University of Cincinnati
231 Albert Sabin Way, Medical Science Building 3109C, Cincinnati,
OH 45267-0514 (USA)
E-mail: kumariha@ucmail.uc.edu

Dr. C. L. Dennis, Dr. S. R. Kline
National Institute of Standards and Technology
100 Bureau Drive, Gaithersburg, MD 20899-8552 (USA)

Dr. A. V. Mossine, Prof. C. A. Deakyne, Prof. J. L. Atwood
Department of Chemistry, University of Missouri-Columbia
601 S. College Avenue, Columbia, MO 65211 (USA)
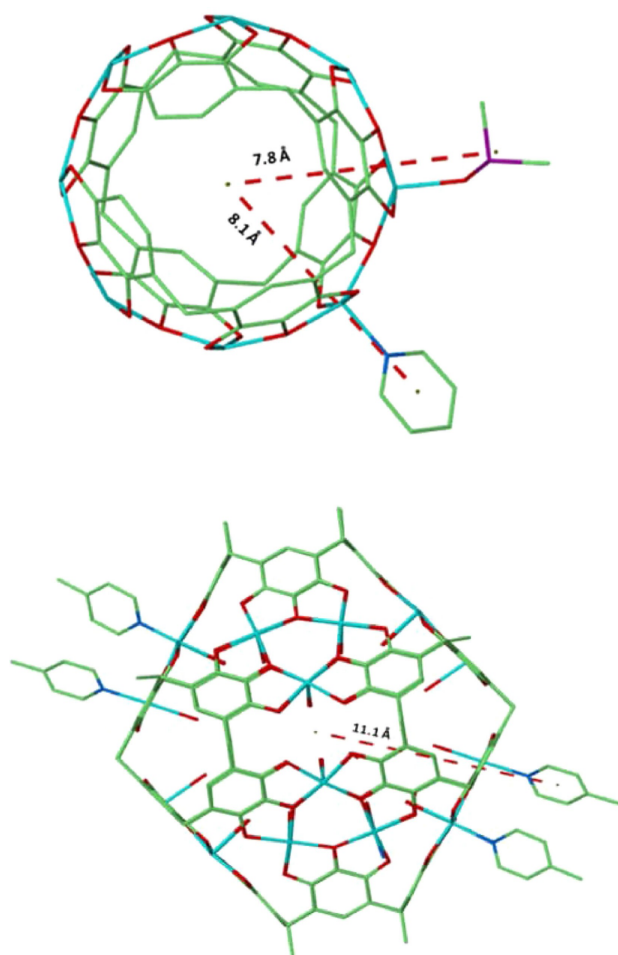E-mail: AtwoodJ@umsystem.edu

Figure 1. Structures determined from X-ray diffraction for *C*-propylpyrogallol[4]arene nickel dimer (top) vs. *C*-propylpyrogallol-[4]arene nickel hexamer (bottom). Radii are indicated with dashed red lines. O: red, Ni: turquoise, C: green, N: blue; S: purple. Hydrogens and most pyridine and DMSO ligands have been removed for clarity.

phase.[14] Our pioneering effort towards studying these properties in solution yielded intriguing information about their solution and magnetic properties.

The initial Superconducting Quantum Interference Device Vibrating Sample Magnetometer [SQUID VSM (21)] measurements on methanol-solubilized PgC$_3$Ni hexamers and dimers between 300 K and 15 K reveal the paramagnetic nature of the MONCs. The magnetization (M) vs. applied magnetic field (H) for both the hexamer and dimer is a straight line that passes through the origin with a positive magnetic susceptibility (Figure 2 top and bottom). (At the lowest temperature of 2 K, the straight-line M vs. H adds an s-shaped component, perhaps indicative of a trend towards magnetic saturation of the nanocapsules; Supporting Information).

Generally, the mass susceptibility increases with decreasing temperature, due to the reduced thermal energy of the
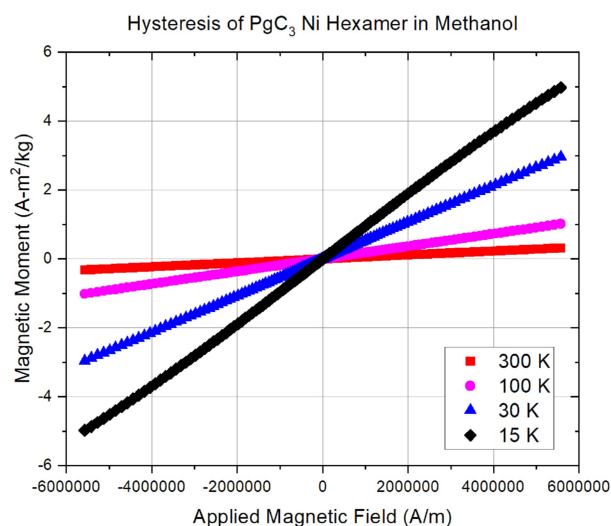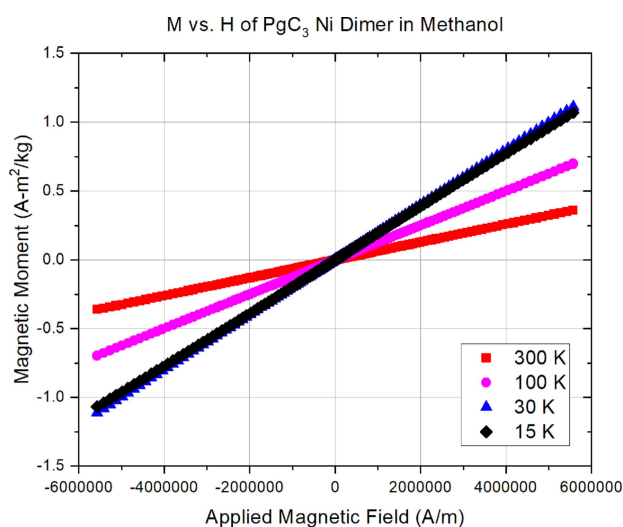

Figure 2. *M* vs *H* curve for *C*-propylpyrogallol[4]arene nickel dimer (top) and *C*-propylpyrogallol[4]arene nickel hexamer (bottom) in methanol at 300 K, 100 K, 30 K and 15 K. Error bars represent 1σ and are shown, but may be smaller than the symbol.

assemblies of radius 10 Å. This solution-phase radius is close to the X-Ray Diffraction (XRD) radius size of 11.1 Å (hexamer centroid···centroid pyridine ligand) (Figure 1, bottom). Parallel to the hexameric measurements, the radius of a dimer as measured from the dimer centroid to the ligand centroid varies between radius 7.8 Å (with a dimethyl sulfoxide [DMSO] ligand) to 8.1 Å (with a pyridine ligand) in the solid state (Figure 1, top). This radius size is close to the observed 7 Å radius of a dimer in methanolic or DMSO solution. The slight differences in sizes of about 1.1 Å for both the hexamer and the dimer between the two phases can be attributed to the presence of ligands and the solvent effect. The close proximity between the two (XRD and SANS) measurements demonstrates the stability of metal-organic nanocapsules (MONCs) in solution.

The magnetic behavior of these MONCs is another important aspect of their eventual applications.[8–13] MONCs not only possess discrete shapes but also have magnetically interesting metals, such as nickel and cobalt, yet their magnetic properties have not been explored in the solution

electrons and the enhanced alignment of the magnetic moments in the direction of the field. Specifically, the mass susceptibility increases from $6.484(1)\times10^{-8}\,\mathrm{m^3\,kg^{-1}}$ at 300 K to $12.2497(1)\times10^{-8}\,\mathrm{m^3\,kg^{-1}}$ at 100 K to $19.965(1)\times10^{-8}\,\mathrm{m^3\,kg^{-1}}$ at 30 K to $19.320(6)\times10^{-8}\,\mathrm{m^3\,kg^{-1}}$ at 15 K for the PgC_3Ni dimer. The mass susceptibility increases from $5.756(3)\times10^{-8}\,\mathrm{m^3\,kg^{-1}}$ at 300 K to $18.203(3)\times10^{-8}\,\mathrm{m^3\,kg^{-1}}$ at 100 K to $53.35(1)\times10^{-8}\,\mathrm{m^3\,kg^{-1}}$ at 30 K to $92.1(1)\times10^{-8}\,\mathrm{m^3\,kg^{-1}}$ at 15 K for the PgC_3Ni hexamer. The net mass susceptibility doubles from 300 K to 100 K and then triples from 300 K to 30 K/15 K for the PgC_3Ni dimer, whereas for the PgC_3Ni hexamer it triples from 300 K to 100 K and then increases by a factor of 10 from 300 K to 30 K and then almost a factor of 20 from 300 K to 15 K. The larger increase in susceptibility with temperature in the hexamer versus the dimer cannot be explained simply by the differences in the coordination environments in the hexamer and dimer.

Therefore, we measured the magnetization as a function of temperature (M vs. T at $H = 400\,\mathrm{kA\,m^{-1}}$) to explore possible interactions between and within the nanocapsules. The curve for the nickel hexamer shows pure paramagnetic behavior (Figure 3, bottom); however, the curve for the nickel dimer shows the presence of an additional feature at around 20 K (Figure 3, top). This intriguing feature at 20 K indicated either possible magnetic interactions or the presence of additional magnetic species, which could also account for the large change in susceptibility with temperature.

SANS measurements were conducted at room temperature (RT) on the NG-7 30-m SANS, NIST Center for Neutron Research, to investigate the presence of entities in solution of the nickel-seamed *C*-propylpyrogallol[4]arene dimer and hexamer (SQUID samples). Samples were prepared in deuterated DMSO or deuterated methanol at a volume fraction of approximately 1 %. The raw SANS data was reduced using standard protocols and analyzed using Igor Pro software at the NCNR.[15] Before fitting model structures to the data, the q-independent incoherent background was subtracted from each data set. Some samples showed an upturn in scattering at low q-values indicating the presence of larger aggregates, but the samples did not flocculate or precipitate with time, If this upturn in the scattering was present, this data range was excluded from the data analysis. The neutron scattering curves were fit to both uni- and bimodal Schulz sphere models to investigate the presence of spherical assemblies in solution. The scattering data for the hexameric assembly fitted well to the unimodal Schulz sphere model (Figure 4, bottom) while that for the dimer fitted to a bimodal Schulz sphere model (Figure 4 top).

The data analysis on SANS revealed the presence of monodisperse spheres of radius 10 Å in the hexamer solution but the presence of spheres of radius 7 Å and 13 Å in the dimer solution. The volume fraction of the 13 Å-radius species was much smaller than that of the 7 Å dimer. Although we have not been successful in isolating crystals of the 13 Å species, this exciting result now gives us a pathway to formation of MONCs even larger than the existing hexamers. Notably, the low q scattering (last few points not
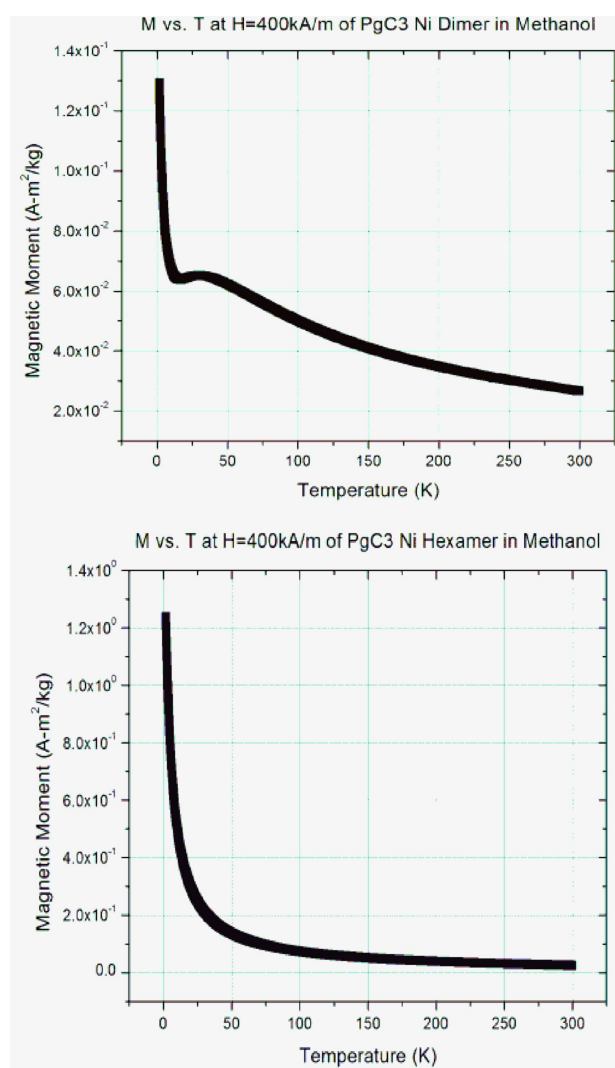

Figure 3. Normalized *M* vs. *T* plots at 400 kA m^{-1} (5000 Oe) for *C*-propylpyrogallol[4]arene nickel dimer (top) vs. *C*-propylpyrogallol-[4]arene nickel hexamer (bottom). Error bars represent 1σ and are shown, but may be smaller than the symbol.

fitted) also suggests presence of some aggregates (see Figure 4).

To further investigate this unprecedented result, we probed deeper by conducting a detailed experimentation on PgC_n–Ni nanocapsules. In our prior mechanistic in situ solution studies on PgC_n metal-seamed nanocapsules, temperature, solvent and type of metal were reported to be the key factors that controlled the equilibrium between hexameric and dimeric nanoassemblies.[10] Later, we reported the role of pH and centrifugation in directing the formation of PgC_nFe nanotubes in solution.[11] Unlike these prior studies which were conducted only in solution to probe equilibrium structures, in this work, we isolated solid-state fractions of PgC_3Ni at various stages of synthesis and studied their magnetic properties. Herein, we determine the magnetic moment from the Quantum Mechanical Langevin fit of the 5 K *M* vs. *H* data and the interaction temperature (which indicates the deviation from pure paramagnetic non-inter-
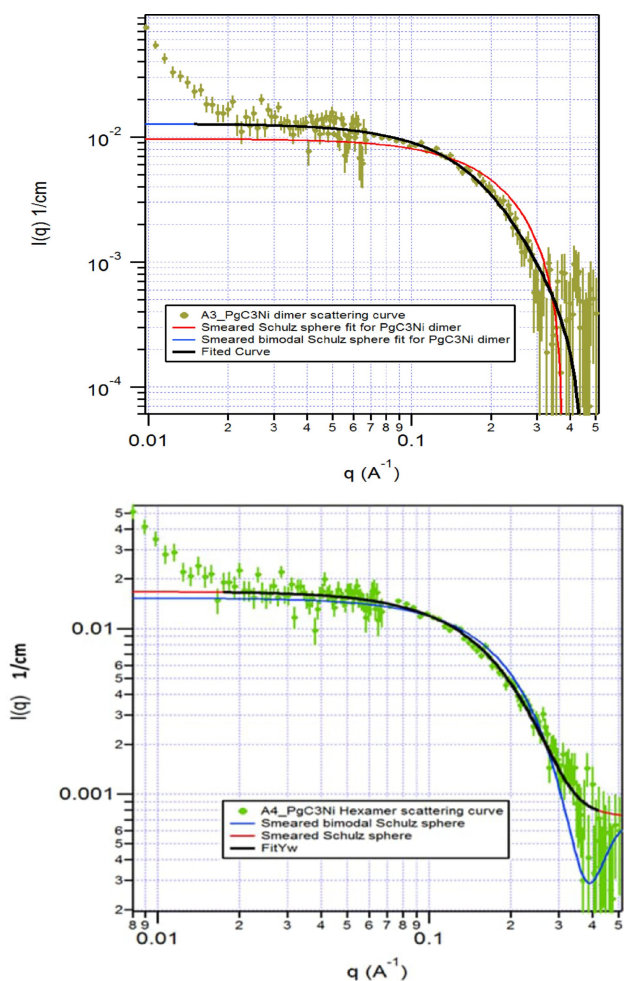
Table 1: Solid-state sample codes along with moment in Bohr magnetons and interaction temperature in Kelvin of PgC$_3$Ni aliquots. Errors are 1σ.

Sample	Code	Moment [μ_B]	T_{int} [K]
Hot Synthesis-DMSO-Crystals	H-D-1	1.675 ± 0.008	-2.3 ± 0.1
Hot Synthesis-DMSO-Filtrate	H-D-2	1.661 ± 0.007	-1.5 ± 0.1
Hot Synthesis-MeOH-Precipitate	H-M-1	1.85 ± 0.01	-1.2 ± 0.1
Hot Synthesis-MeOH-Filtrate	H-M-2	1.74 ± 0.02	-1.19 ± 0.05
RT Synthesis-DMSO-Crystals	R-D-1	1.94 ± 0.01	-0.90 ± 0.03
RT Synthesis-DMSO-Filtrate	R-D-2	1.81 ± 0.03	-0.2 ± 0.2
RT Synthesis-MeOH-Precipitate	R-M-1	2.15 ± 0.01	-1.99 ± 0.08
RT Synthesis-MeOH-Filtrate	R-M-2	1.567 ± 0.008	-1.24 ± 0.02

PgC$_3$Ni hexamer to be (1.68 ± 0.01) μ_B and (-2.26 ± 0.04) K, respectively. Pure PgC$_3$Ni dimer had a comparable moment of (1.65 ± 0.01) μ_B, but a lower T_{int} of (-1.0204 ± 0.0002) K.

In the case of the hot synthesis in DMSO, the moment and T_{int} of the first aliquot (H-D-1) are in excellent agreement with those of a hexamer; however, the second aliquot (H-D-2) is more similar to a dimer with a comparable moment and slightly higher T_{int} (Table 1). The solution-phase geometries/SANS results for H-D-1 (hexamers) and H-D-2 (mostly dimers) agree with the solid-state behavior (magnetic data). Interestingly, the hot synthesis in methanol yielded the first aliquot (H-M-1) with a higher moment and intermediate T_{int} than those reported earlier for a pure hexamer and dimer, suggesting the presence of a mixture and/or some higher-order species. SANS analyses of H-M-1 indicate the presence of a cylindrical species of $R = 11$ Å (Table 2), consistent with the discrepancy in the magnetic data with respect to that for a typical dimeric/hexameric sphere. Note that T_{int} of this 11 Å cylindrical tube is -1.2 K which is comparable to the iron-seamed pyrogallol[4]arene nanotube[11] (-1.14 K) but not to that of the ferrocene-enclosed pyrogallol[4]arene nanotube[16] (-0.5 K), suggesting that Ni is seaming the nanotubular framework for H-M-1 (Figure 5, left).

Similarly, the second aliquot (H-M-2) has a higher moment and an intermediate T_{int} (between that of the hexamer and the dimer). These results again suggest the possible presence of multiple species (hexamer, dimer, and another species). SANS analyses of H-M-2 indicate the presence of the dimer, hexamer, and a higher-order spherical species ($R = 13$ Å; Figure 6). Notably, the presence of higher-order species in the H-M solid-state samples is in agreement with the solution-phase SANS and solution-phase magnetic results discussed earlier in this paper.

For the room temperature-DMSO synthesis, the first aliquot (R-D-1) has a moment higher than those of pure PgC$_3$Ni hexamer and dimer, but T_{int} was slightly lower than that of pure dimer which suggests the presence of dimer and higher-order spherical species. SANS fitting with a bimodal Schulz sphere model for R-D-1 confirms the presence of dimer and 13 Å-radius species in solution. To our surprise, the second aliquot (R-D-2) showed a T_{int} value similar to that of a pure paramagnet, suggesting the presence of either unreacted material or of Ni within the nanoassembly at non-interacting distances. SANS analyses of R-D-2 show the

Figure 4. Uni- and bi-modal Schulz sphere fits for *C*-propylpyrogallol-[4]arene nickel dimer solution (top) and *C*-propylpyrogallol[4]arene nickel hexamer solution (bottom). Error bars represent 1σ and are shown, but may be smaller than the symbol.

acting behavior; aka ferromagnetic or antiferromagnetic interactions between the magnetic atoms) from a modified Curie–Weiss fit of the M vs T data (see Supporting Information). We then compare the moment and characteristic interaction temperature of the various aliquots with our previously reported magnetic work on pure PgC$_3$Ni dimer and hexamer. We also investigated these fractions in solution using SANS.

For this study, we chose temperature and solvent as the two key variables to prepare and investigate various fractions of PgC$_3$Ni nanocapsules. Syntheses were conducted in DMSO and methanol at RT and near solvent boiling temperatures (Hot Synthesis). For each condition (temperature and solvent) an initial fraction of crystals/precipitate was separated from the supernatant. A second fraction of crystals/precipitate was obtained by adding water to the resultant filtrate. For ease, we will refer to the codes enlisted in Table 1 for these aliquots. The measurements were performed on a SQUID magnetometer, with M vs. H at 5 K and 300 K and M vs. T under a field of 16 kA/m. In our prior study, we reported the moment and T_{int} for a pure

Angew. Chem. Int. Ed. **2022**, *61*, e202203010 (4 of 6)

© 2022 The Authors. Angewandte Chemie International Edition published by Wiley-VCH GmbH

Table 2: Summary of speciation results from SQUID and SANS.[a]

Sample	Code	Resultant Species
Hot Synthesis-DMSO-Crystals	H-D-1	Hexamer ($R = 9.84$ Å)
Hot Synthesis-DMSO-Filtrate	H-D-2	Mostly dimers ($R = 7$ Å)
Hot Synthesis-MeOH-Precipitate	H-M-1	Cylinder (11 Å)
Hot Synthesis-MeOH-Filtrate	H-M-2	Mostly dimers, hexamers, sphere ($R = 13$ Å)
RT Synthesis-DMSO-Crystals	R-D-1	Dimers, sphere ($R = 13$ Å)
RT Synthesis-DMSO-Filtrate	R-D-2	Sphere ($R = 8$ Å)
RT Synthesis-MeOH-Precipitate	R-M-1	Sphere ($R = 13$ Å)
RT Synthesis-MeOH-Filtrate	R-M-2	Mostly dimers

[a] The word "mostly" refers to the higher volume fraction species confirmed by both SANS and SQUID measurements. Fitted polydispersity for the radius was typically 0.2. Details are in the Supporting Information.
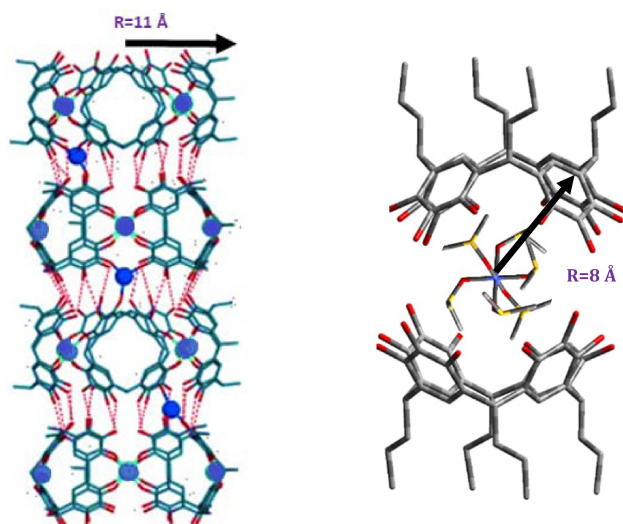

Figure 5. Left: Proposed structure of the 11 Å cylinder (H-M-1) showing how metal centers seam the framework. H-bonds are indicated with dashed red lines. O: red, Ni: blue, C: green. Hydrogens and most pyridine and DMSO ligands have been removed for clarity.; Right: Proposed structure of the 8 Å spherical species (R-D-2) showing the presence of a metal-solvent complex in the center. O: red, Ni: purple, C: grey. Hydrogens have been removed for clarity.
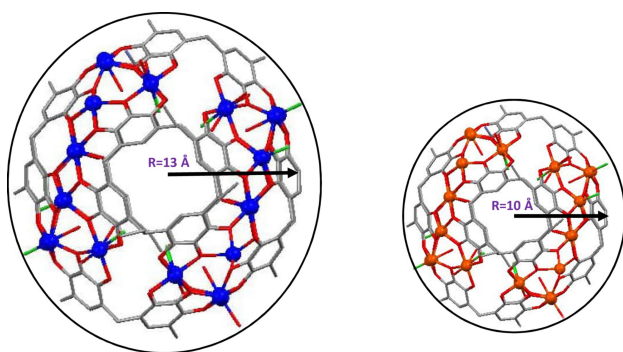

Figure 6. Left: Proposed structure of 13 Å metal-seamed spheres with both octahedral and square planar metal centers.; Right: 10 Å X-ray diffraction structure of PgCnM hexamer. O: red, Ni: purple, C: grey. Hydrogens have been removed for clarity

presence of an 8 Å-radius sphere, one that may have Ni atoms in the cavity rather than the framework (similar to Co/Mn enclosed RsCn dimers; Figure 5, right)[17] to yield the much lower T_{int} (-0.2 K) but higher moment (1.81 μ_B). Note that the moment of the Ni complexes varies with the environment as well as the oxidation state.[18] Specifically, Ni complexes can be square planar with no unpaired electrons (0 μ_B) or octahedral with two unpaired electrons (2.83 μ_B). However, when in a coordinating solvent, the magnetic moment can be intermediate between the values, depending on the impact of the ligand. Alternatively, a mixture of oxidation states Ni^{+2} (max 2.83 μ_B) and Ni^{+3} (max 1.7 μ_B), can also result in a magnetic moment intermediate between the two values. In this case, the simplest explanation that matches the data is a mixture of (approx. 40%) square planar and (approx. 60%) octahedral states of Ni^{+2}, which is the hypothesized structure in Figure 5.

The RT synthesis in methanol yielded the aliquot (R-M-1) with the highest moment of 2.15 μ_B, suggesting the presence of a 13 Å-radius spherical species that is structurally similar to the hexamer (1.68 μ_B), but with different ligand interaction within the Ni complex resulting in a shift of the magnetic moment closer to the 2-unpaired electron value (Figure 6). The T_{int} of R-M-1 (-1.99 K) is only slightly lower than that of a pure PgC_3Ni hexamer (-2.3 K) due to some changes in the antiferromagnetic interactions likely due to the increased spacing or the differences in the coordinating environment. The second aliquot (R-M-2) for the RT synthesis in methanol yielded a moment and T_{int} values close to that of a dimer. SANS data analyses for R-M-1 and R-M-2 align with the speciation results from the magnetic data. Overall, the 13 Å-radius species is observed primarily in RT synthesis aliquots of DMSO and methanol, further affirming our prior finding that low temperatures favor the self-assembly of larger hexameric species.[10]

In conclusion, these measurements give the first indication of the presence of a species with an internal volume about twice that of a hexamer. This larger species is important not only because it extends the size of nanocapsules available as reaction vessels but also because it shows that other geometric arrangements are possible for these macrocycles. The mechanistic study further confirms the presence of higher-order species ($R = 13$ Å) with both octahedral and square planar Ni centers in methanolic solid-state samples at both temperatures and DMSO samples at

RT. These results agree with solution-phase SANS and magnetic results. Two additional new species were also identified: a) Cylinders in hot methanolic synthesis (ppt) with Ni centers seaming the framework and b) spheres ($R = 8$ Å) with non-interacting Ni metals (possibly within the internal cavity of the capsules). This mechanistic study paves a pathway to isolate select nanocontainers for specific applications.

Acknowledgements

Conflict of Interest

The authors declare no conflict of interest.

Data Availability Statement

The data that support the findings of this study are available in the Supporting Information of this article.

[1] Y. Cohen, T. Evan-Salem, L. Avram, *Supramol. Chem.* **2008**, *20*, 71–79.

[2] S. Slovak, T. Evan-Salem, Y. Cohen, *Org. Lett.* **2010**, *12*, 4864–4867.

[3] C. Wang, E. Wyn-Jones, K. C. Tam, *Colloids Surf. A* **2010**, *364*, 49–54.

[4] T. Imae, *J. Colloid Interface Sci.* **2000**, *225*, 285–290.

[5] H. Kumari, C. A. Deakyne, J. L. Atwood, *Acc. Chem. Res.* **2014**, *47*, 3080–3088.

[6] "Small-Angle Neutron Scattering in Supramolecular Complexes": H. Kumari, *Comprehensive Supramolecular Chemistry II*, Elsevier, Amsterdam, **2017**, pp. 289–302.

[7] H. Kumari, A. V. Mossine, S. R. Kline, C. L. Dennis, D. A. Fowler, C. L. Barnes, S. J. Teat, C. A. Deakyne, J. L. Atwood, *Angew. Chem. Int. Ed.* **2012**, *51*, 1452–1454; *Angew. Chem.* **2012**, *124*, 1481–1483.

[8] A. Morelos-Gómez, F. López-Urías, E. Muñoz-Sandoval, C. L Dennis, R. D. Shull, H. Terrones, M. Terrones, *J. Mater. Chem.* **2010**, *20*, 5906–5914.

[9] C. W. Evans, C. L. Raston, K. S. Iyer, *Green Chem.* **2010**, *12*, 1175–1179.

[10] L. Bogani, W. Wernsdorfer, *Nat. Mater.* **2008**, *7*, 179–186.

[11] H. Kumari, S. R. Kline, C. L. Dennis, A. V. Mossine, R. L. Paul, C. A. Deakyne, J. L. Atwood, *Angew. Chem. Int. Ed.* **2012**, *51*, 9263–9266; *Angew. Chem.* **2012**, *124*, 9397–9400.

[12] H. Kumari, C. L. Dennis, A. V. Mossine, C. A. Deakyne, J. L. Atwood, *J. Am. Chem. Soc.* **2013**, *135*, 7110–3.

[13] H. Kumari, C. L. Dennis, S. R. Kline, A. V. Mossine, C. A. Deakyne, J. L. Atwood, *ACS Nano* **2012**, *51*, 1452–1454.

[14] J. L. Atwood, E. K. Brechin, S. J. Dalgarno, R. Inglis, L. F. Jones, A. Mossine, M. J. Paterson, N. P. Power, S. J. Teat, *Chem. Commun.* **2010**, *46*, 3484–3486.

[15] S. R. Kline, *J. Appl. Crystallogr.* **2006**, *39*, 895–900.

[16] A. V. Mossine, H. Kumari, D. A. Fowler, A. Shih, S. R. Kline, C. L. Barnes, J. L. Atwood, *Chem. Eur. J.* **2012**, *18*, 10258–10260.

[17] A. M. Drachnik, H. Kumari, C. L. Barnes, C. A. Deakyne, J. L. Atwood, *CrystEngComm* **2014**, *16*, 7172–7175.

[18] B. N. Figgis, *Introduction to Ligand Fields*, Wiley, New York, **1966**.